WPMST1-PR(18) 20564

F Felici et al.

Model-based design, simulation and testing of an electron temperature profile controller on ASDEX-Upgrade

Preprint of Paper to be submitted for publication in
Nuclear Fusion

This work has been carried out within the framework of the EUROfusion Consortium and has received funding from the Euratom research and training programme 2014-2018 under grant agreement No 633053. The views and opinions expressed herein do not necessarily reflect those of the European Commission.

Model-based design, simulation and testing of an electron temperature profile controller on ASDEX-Upgrade

F. Felici[1*], O. Kudlacek[2], T. Ravensbergen[3], W. Treutterer[2], T.C. Blanken[1], A. Teplukhina[4], O. Sauter[4], B. Geiger[2], L. Giannone[2], M. Reich[2], J. Stober[2], M. Willensdorfer[2], the ASDEX-Upgrade Team[2] and the EUROFusion MST1 Team[5]

[1]Eindhoven University of Technology, Department of Mechanical Engineering, Control Systems Technology Group, P.O. Box 513, 5600MB, Eindhoven, The Netherlands
[2]Max-Planck Institut für Plasmaphysik, Boltzmannstrasse 2, 85748 Garching, Germany
[3]DIFFER - Dutch Institute for Fundamental Energy Research, De Zaale 20, 5612AZ Eindhoven, The Netherlands
[4]École Polytechnique Fédérale de Lausanne (EPFL), Swiss Plasma Center (SPC), CH-1015 Lausanne, Switzerland
[5]See the authorlist of H. Meyer et al 2017 Nucl. Fusion 57 102014
[*]Present address: SPC/EPFL[4].

E-mail: *federico.felici@epfl.ch

Abstract. A model-based, multivariable feedback controller to control the electron temperature profile using Electron Cyclotron Resonance Heating (ECRH) power has been designed and tested on the ASDEX-Upgrade tokamak. First, the control-oriented nonlinear plasma simulator RAPTOR was used to reproduce the time-evolution of the kinetic profiles for the target discharge. Then, a controller was designed based on a linearization of this RAPTOR simulation. The controller was then tested in closed-loop simulations, again using RAPTOR as a plasma simulator, followed by implementation in the ASDEX-Upgrade discharge control system and testing in the experiment. Already during the first test discharge, the controller performed as expected from simulations, allowing the temperature profile to be maintained constant during a change from off-axis to on-axis NBI heating within the limits of actuator saturation. This work represents an example of a controller design paradigm for next-generation tokamak operations, where it will be increasingly important to design controllers based on simulations in order to minimize the experimental time used for controller tuning.

31 July 2018

1. Introduction

Model-based control design is the leading paradigm for improving the performance of modern high-technology systems, and fusion devices are no exception.

In model-based control design, a *control model* is used to design and test a controller before deploying it on the actual system. This control model has to be sufficiently complex to capture the main (dynamic) relationship between the inputs (actuators) and outputs (plasma quantities to be controlled), yet in a suitable mathematical form that allows controller design, and computationally tractable to allow rapid design iterations. As understanding of tokamak physics progresses and models become more accurate, and computing power increases allowing more complex behaviour to be simulated, more and more aspects of tokamak control become amenable to model-based control design.

In the past decades, applications of model-based control have ranged from magnetic control of position and plasma shape [1], to Resistive Wall Mode control [2], profile control [3, 4, 5] and burn control [6]. This is in contrast with traditional practices of manual tuning of (PID)

controller gains based on experimental trials. Indeed, controller design and validation for next-generation tokamaks like ITER, where experimental time is particularly scarce and expensive, is expected to strongly rely on model-based methods [7, 8].

In this paper we present a practical example of this approach for the design of a multivariable electron temperature T_e profile controller for the ASDEX-Upgrade tokamak. This MIMO (Multi-Input-Multi-Output) controller controls multiple (in this case, two) principal directions of the profile using two independent ECRH sources, aimed at different radial locations. We show that, by following a systematic model-based design procedure, it was possible to obtain a controller that performed as expected from closed-loop simulations on its very first experimental test. This also represents, to the best of our knowledge, the first time that the T_e *profile* on a tokamak was successfully controlled in feedback‡.

Such a T_e controller is useful for a variety of physics applications. One of them, that was the focus of the particular experiments described in this paper, is to keep the temperature profile constant while changing heating and current drive sources. This helps to maintain a constant shape of the ohmic component of the current density profile, thereby facilitating the analysis of the experiment. Other useful applications may include detailed studies of turbulent transport under constant temperature gradients.

Various approaches to model-based profile control that have recently been investigated differ in the way the control model has been obtained, and also in the control method used. For example, [10] derives a control model represented by a set of linear ODEs from experimental data: system identification experiments are carried out on the tokamak to be controlled around an operating point, and a model is fitted to match the experimental behaviour. More recently, there have been examples where a linear model is derived from system identification based on simulation data from tokamak profile simulation codes like TRANSP [11] or METIS [3]. Alternatively, first-principle-based control-oriented models have been used to derive current profile controllers [4, 5].

Controllers applied to profile control range from Singular-Value-Decomposition based controllers [4], [12] to Model-based Predictive Controllers [13], [5] and various approaches originating from nonlinear control [14, 15, 16]. In this work, a linear model used for controller design is obtained from the control-oriented plasma transport simulator RAPTOR [17]. Additionally, RAPTOR acts as nonlinear plasma simulator to test the controller in closed-loop simulations. A useful feature of RAPTOR is that the linearized model (a set of linear Ordinary Differential Equations (ODEs)) describing the variation of the plasma states around an operating point is obtained automatically from the solution of the (nonlinear) transport equations, which obviates the need for system identification procedures to extract a linearized model. This feature was previously used in model-based predictive control of the current profile on TCV [5].

Another important feature that distinguishes this controller from previous work is in the way the to-be-controlled T_e profile is estimated in real-time. Instead of controlling the T_e profile based on a dedicated diagnostic measurement, this profile is obtained from a real-time state estimation algorithm that merges several measurements of the plasma with real-time model predictions into a single estimate of the plasma profiles. This state reconstruction algorithm is known as a *dynamic state observer*, and since its internal model relies on a real-time implementation of the already mentioned RAPTOR code used for simulation, it is known as the RAPTOR-observer. Using an observer, rather than directly relying on diagnostic data, carries several advantages as discussed in e.g. [18]. Of particular use in this T_e control application is the ability to make the controller independent from the details of the diagnostic being used to gather information about the to-be-controlled profile. Another advantage in this context is the natural ability to discard unreliable diagnostic measurements that are clearly incompatible with the values predicted from the model, increasing the accuracy and reliability of the profile estimate.

‡ Very recent work [9] shows preliminary results towards achieving T_e profile control on KSTAR using a similar method.

The remainder of this paper is organized as follows: Section 2 describes the setup of the experiments: the plasma scenario for which the temperature is to be controlled, as well as the implementation of the real-time state reconstruction and control algorithms on the ASDEX-Upgrade control system. Section 3 details the steps of designing and testing the controller starting from a RAPTOR simulation of the target discharge, proceeding with derivation of the linear model and finally design and testing of the controller. Section 4 shows the experimental results of using the controller on the first plasma shot, demonstrating the performance expected from simulations.

2. Plasma scenario and control system components

2.1. Plasma scenario

The need to design a T_e profile controller came out of a set of experiments carried out at ASDEX-Upgrade to study the efficiency of on-axis and off-axis neutral-beam driven current in various situations. As described in [19], these experiments featured pre-programmed switches between periods of on-axis Neutral Beam Injection (NBI) current drive and off-axis NBI current drive. To facilitate the study of the change of the neutral beam driven current when switching from on-axis heating to off-axis heating, constant electron temperature profiles were required to keep the profile shape of the ohmic current and bootstrap current constant. In some cases, temperature feedback control was done using a single ECRH source, feeding back the measurement from a single, pre-selected ECE channel measuring the radiation temperature at the desired radial position. While this feedback was relatively successful, it required some trial and error to get the desired results and, while the temperature at a given location could be kept constant, it was obviously not possible to match the entire profile with a single-input-single-output (SISO) controller. An example thereof is shown in Figure 1.

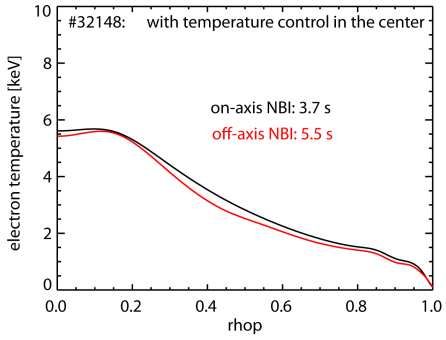

Figure 1. Temperature profiles obtained during a previous shot using SISO temperature control (AUG#32148), as reconstructed by IDA [20]. This motivates the positioning of one ECRH source at $\rho_{pol} = 0.4$ to compensate for the profile mismatch.

To compensate for this mismatch in temperature, a new ECRH distribution is designed, to be used in the MIMO feedback control experiments. One ECRH beam, to be controlled in feedback, was aimed at $\rho_{\mathrm{pol}} = 0.4$, corresponding to the location of the T_e mismatch observed in Figure 1. The other feedback controlled source was aimed at $\rho_{\mathrm{pol}} = 0.2$. Another source, controlled only in feedforward, was aimed at a similar location close to the axis for avoiding core impurity accumulation and another off-axis for NTM avoidance and stabilization purposes. The ECRH beam setup, as designed for the new experiments to be carried out with the MIMO controller, is shown in Figure 2

2.2. Control system components

2.2.1. Real-time diagnostics and data processing algorithms ASDEX-Upgrade has an extensive set of real-time diagnostics whose data is sent to and processed by the Discharge

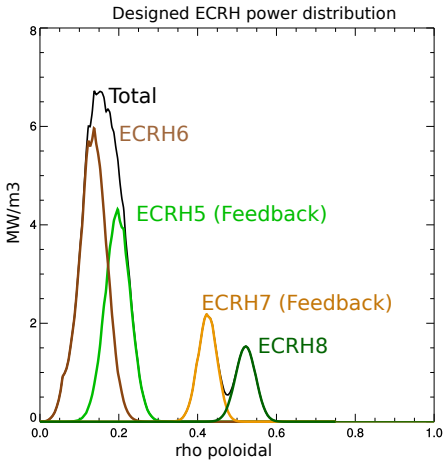

Figure 2. ECRH beam deposition locations, computed using the TORBEAM code based on a previous AUG equilibrium (#33864, $t = 5.5$s). Only ECRH 5 and 7 will be controlled in feedback.

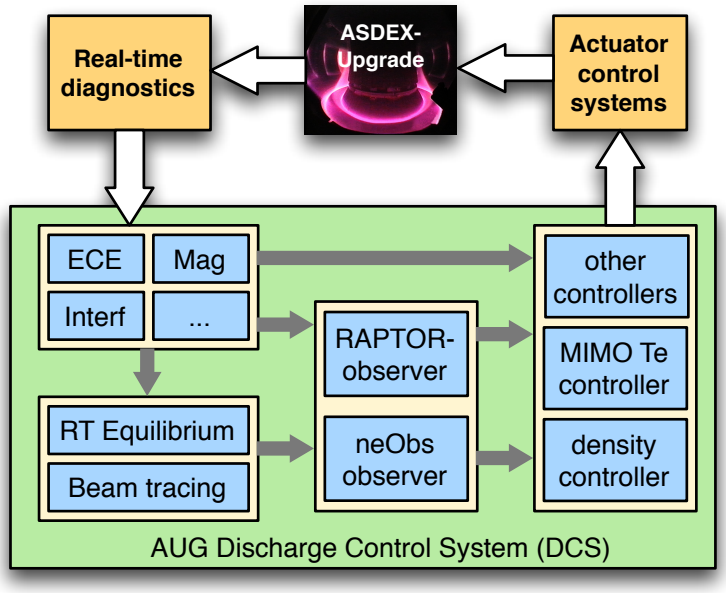

Figure 3. Block diagram showing the main components of the control loops described in this paper. Real-time diagnostic signals, equilibrium information and real-time ray tracing information are fed to state observers that calculate an estimate of the plasma profiles. The T_e profile estimate from the RAPTOR-observer is fed to the MIMO T_e controller, while the density profile estimate is fed to a density controller.

Control System (DCS) [21]. For the work described in this paper, the real-time Electron Cyclotron Emission (ECE) diagnostic is particularly important, as it is used to constrain the estimate to-be-controlled T_e profile estimate. A real-time data analysis software takes 6ms to simultaneously analyze the correlation of ECE channels to magnetic probe signals to detect Neoclassical Tearing Modes [22] as well as return a time-averaged T_e value. Simultaneously, magnetic signals are fed to a real-time Grad-Shafranov reconstruction code [23] which calculates the equilibrium in real-time.

2.2.2. RAPTOR observer As mentioned in the introduction, the T_e profile controller does not directly use temperature measurements, but relies on a real-time profile estimate from the RAPTOR-observer [18, 24]. This receives information from multiple real-time diagnostics and algorithms to compute an optimal real-time estimate of the plasma states, in this case the T_e and current density profiles, merging model predictions with diagnostic measurements. The model predictions are obtained by solving the nonlinear, coupled PDEs of poloidal flux diffusion and electron temperature transport. Details of the RAPTOR implementation of these equations can be found in [17], [25]. In this work, the ad-hoc Bohm-GyroBohm model [26] was used as transport model for the electrons, which proved sufficient for our purposes as we shall see.

The state observer also receives information about the plasma equilibrium geometry from the real-time Grad-Shafranov equilibrium reconstruction code. Also, it receives a plasma density profile estimate from the neObs observer based on [27], plasma current measurements and heating powers for all the actuators. The core of the observer algorithm is based on an Extended Kalman Filter [28, 24]. The algorithm executes with step times of 6ms, which is more than sufficient considering AUG's confinement time of > 50ms. For the present application of reconstructing the T_e profile, it suffices to know that the algorithm relies on the real-time ECE diagnostic [29], when available, and supplements this data with the internal transport model in the regions where there are no measurements. For this purpose, 60 channels from the ECE diagnostic are acquired at 1MHz, time-averaged and downsampled to 6ms. Channels that are too close to the plasma edge, or that give unrealistic values compared to the model-based expectations, are automatically discarded by the algorithm. Furthermore, it is assumed that the measured ECE radiation temperature corresponds to the electron temperature in the region of interest, which is a reasonable assumption for core ECE measurements in these plasmas. An H-mode pedestal is also included in the model, and set to 500eV at $\rho_{\text{tor}} = 0.88$ to match experimental observations for these discharges..

2.2.3. Controllers in DCS and limit handling Controllers in DCS are implemented in a dedicated algorithm framework. Actuator limits, both in value and in ramp-rate, are handled by the framework, providing the true actuator output as feedback signal to the controller. This is important for anti-windup purposes, i.e. to ensure that the output calculated by the controller remains close to the actual command sent to the actuators. The controller in this experiment is based, as we shall see, on a MIMO state-space controller. The required matrix operations were implemented in the DCS framework and controller matrices can be passed to the algorithm via a configuration script.

Since the gyrotrons used in this experiment allow only on-off power commands, the continuous power request from the controller is translated to on-off modulation signals by a Pulse Width Modulation (PWM) algorithm. This algorithm has a baseline period of 16ms, with on-off switching occurring at most every 1ms.

2.2.4. Total delays For any feedback loop, it is crucial to consider all delays in the controller design. Based on the knowledge of the control system components, the delays are listed in Table 2.2.4. If the delays are significant with respect to the typical time scales of the system that we are trying to control, they will limit the achievable control bandwidth. For our case, estimating the reaction time of the temperature profile to a fraction of the confinement time (~ 50ms for AUG H-modes), it appears that these delays need to be considered in design of the feedback controller.

Component	**Delay**
ECE data analysis and averaging	6ms
RAPTOR-observer	6ms
Controller	1ms
PWM	1ms
total	14ms

Table 1. Delay budget for T_e profile control loop.

3. Model-based design and testing of the controller

3.1. Model-based controller design procedure

In Figure 4, the steps to obtain the controller are visualised. The procedure is general and essentially holds for any model-based controller design for similar situations.

- We start from a discharge representative of the plasma to be controlled (in terms of density, temperature..), for which there exists a well-analyzed and validated reconstruction of the core profiles. For the shots described here, a TRANSP [30] interpretative simulation was available in which fits of the core kinetic profiles, obtained using IDA [20], were used as input.
- The free parameters in RAPTOR are adjusted so that the RAPTOR predictive profile simulation matches the profiles from TRANSP. This provides the reference control-oriented profile simulation on which to base the controller design.
- The (nonlinear) RAPTOR simulation also yields a set of local linear dynamic models around the trajectory that the nonlinear simulation follows in the plasma state space. This linear model describes, for a chosen time point in the simulation, the perturbed response of the plasma profiles around the trajectory, that would result from a perturbation of the actuator inputs.
- A linear controller (a controller formulated as a set of linear ODEs) is designed using the established control synthesis techniques, and tested in closed-loop with the linearized model.
- When the testing on the linear model gives satisfactory closed-loop behaviour, the controller is tested in closed-loop using RAPTOR as a (nonlinear) plasma simulator to verify that the closed-loop behaviour is still correct in the presence of nonlinearities.
- The linear controller is implemented in the control system software and is tested in open-loop to ensure that the implementation behaves correctly.
- Finally, the controller is tested in closed-loop in a plasma experiment - using the output of the controller to affect a plasma actuator. If the results are significantly different from what was expected from the model, further iterations of any of the previous steps can be carried out.

In the following sections, we go into more detail on these steps as followed for this particular controller design.

3.2. Control-oriented modelling of the target discharge

When using RAPTOR as a control-oriented plasma simulator (and not as first-principles simulator of the plasma), it is perfectly acceptable that some quantities need to be externally fed to RAPTOR, and some parameters have to be manually set to simulate a given class of discharges.

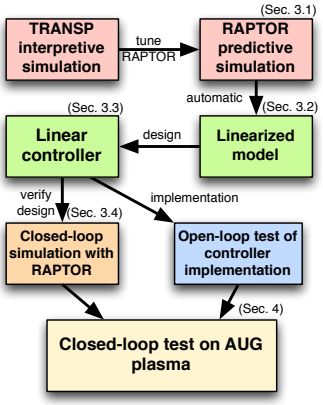

Figure 4. Illustration of the systematic procedure followed to design and test the controller based entirely on models. Note the hierarchy of codes and models employed, from more complete TRANSP analysis, to control-oriented simulator like RAPTOR, to linear models used for control design.

For this work, we use ECRH and NBI deposition profiles taken from TRANSP, as well as the density profile evolution and total plasma current. The equilibrium geometry was taken from a standard AUG discharge with similar plasma volume, and kept fixed for the RAPTOR simulation. RAPTOR simulates the q profile as well as T_e and T_i profiles, with transport coefficients computed by the Bohm-Gyrobohm transport model [26]. With minimal tuning of transport parameters it was possible to reproduce the electron temperature profile evolution.

The results of the profile evolution matching can be seen in Figure 5. The electron temperature profile is reproduced well, while the global trend of the ion temperature evolution is also recovered (but no quantitative match is obtained). Given that the current sources and total plasma current are the same, it is not surprising that the current density profiles also matches the TRANSP result relatively well.

Following the successful reproduction of the reference discharge, the RAPTOR ECRH settings were changed to reflect the new ECRH deposition location settings described in 2. Now, we have available a (nonlinear) profile evolution simulator that takes as inputs the time-varying power to the various ECRH sources, and returns the time-evolution of the T_e, T_i and q profiles, as well as related profiles of conductivity, bootstrap current, ECRH deposition profiles, thermal diffusion coefficients, and other quantities that are commonly outputs of a transport simulation. The RAPTOR simulation of an entire AUG plasma ($\sim$10s) on an average desktop computer takes a few tens of seconds to complete.

3.3. Linearized model for controller design

The next step is to design a feedback controller that takes the electron temperature profile as input, and returns the ECRH power commands to achieve a target profile. Since the goal is to maintain a constant electron temperature, we will design the controller based on a linearization of the system's response around that operating point. While it is acknowledged that the true dynamic response of the profile to actuator power changes are nonlinear, we will assume a-priori that a linear controller will still be effective, and will check this assumption in hindsight by nonlinear simulations. In fact, an effective (linear) feedback controller will maintain the plasma close to the operating point, in the region where the linear response model is expected to be accurate. We choose to keep the ECRH deposition locations constant in this experiment, since varying the ECRH deposition locations as part of the feedback loop would introduce an important additional nonlinear dependence in the plasma response.

To design and test the controller, the linearization of the plasma response is taken at $t = 4$s, just before the switch from on to off-axis NBI power. Let $\bar{T}_e$ be the vector of electron

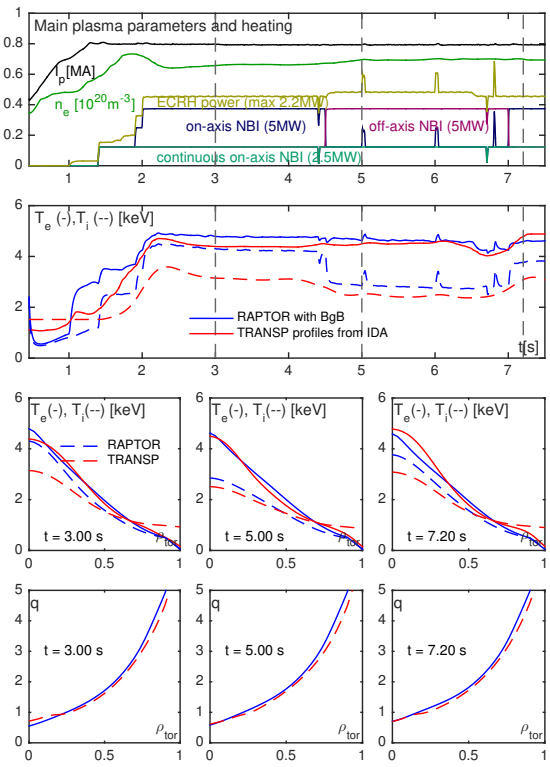

Figure 5. Comparison of an interpretative TRANSP simulation of shot #33864 with RAPTOR predictive profile evolution simulation outputs. Top: density, I_p and auxiliary input power evolution. Second panel: Central T_e and T_i values for TRANSP vs. RAPTOR. Lower panels: $T_e(\rho_{\mathrm{tor,N}})$ and $q(\rho_{\mathrm{tor,N}})$ profile evolution. RAPTOR matches TRANSP results well throughout the flat-top, with some discrepancy in the central ion temperature during the on-axis NBI phase

temperature profile evaluated on a given ρ_{tor} grid (taken with 11 points in this case) and $\bar{P}_{EC}$ the vector of (two) feedback controlled ECRH source powers. At the time of linearization, the plasma has a temperature profile $T_e^o(\rho)$ and corresponding vector with discrete points $\bar{T}_e^o$, as well as ECRH actuator inputs $\bar{P}_{EC}^o$.

The linearized model is written in discrete-time state-space form

$$x_{k+1} = Ax_k + Bu_k \tag{1}$$
$$y_k \quad = Cx_k + Du_k \tag{2}$$

Here, k represents the time index, where a fixed sample time of 1ms was chosen. $y_k = \bar{T}_{e,k} - \bar{T}_e^o$ is the vector of *variation* of electron temperature at time $t = t_k$ with respect to the operating point profile T_e^o, and u_k is the variation of the ECRH power at time t_k w.r.t. the linearization value: $u_k = \bar{P}_{EC,k} - \bar{P}_{EC}^o$. x_k represents the linearized system's internal state. Details on how this linearized model is obtained from the output of the nonlinear RAPTOR simulation are discussed in [17], but it is important to note that the model is obtained directly through an analytical linearization of the nonlinear equations describing the time-evolving coupled system of PDEs, and does not need further iteration or processing of the simulator results. In contrast, the approach presented in [3] requires several nonlinear simulations followed by a system identification procedure to determine a linearized model for controller design.

3.4. Controller design and off-line tuning

With the linearized model available, various control synthesis methods are available for designing a feedback controller. This controller should receive y_k as input and return u_k

for the next time step. In this work, we choose to design a Singular Value Decomposition (SVD)– based decoupling controller, which is a common approach for profile controller design and was followed also in [12] and [31] for q profile control. We summarize the design here, and details can be found in Appendix A.

The starting point for the controller is the DC gain (or steady-state response matrix) of the linearized model. This matrix is first scaled and inputs/outputs are weighted to reflect their importance in the control. Then, an SVD of the resulting scaled and weighted matrix is taken, which gives the principal input-output directions of the system, i.e. the directions of the output vector space that can best be controlled by the actuators. Since we have only two actuators and 11 outputs (11 radial points in T_e), it will be possible to control only two directions of the output, reflected by the first two output singular vectors. These vectors are plotted in 6. As expected, the first singular vector represents a bulk variation in the profile, while the second represents a higher-order profile shape variation. The corresponding input directions (directions in the 2D input vector space) are also shown, describing the linear combination of actuator powers needed to control these output directions§.

We then design two separate PI controllers for each of the principal directions and tune the gains manually to achieve a desired closed-loop response. In this tuning, known delays are also taken into account as they restrict the closed-loop bandwidth (the response speed) of the controller.

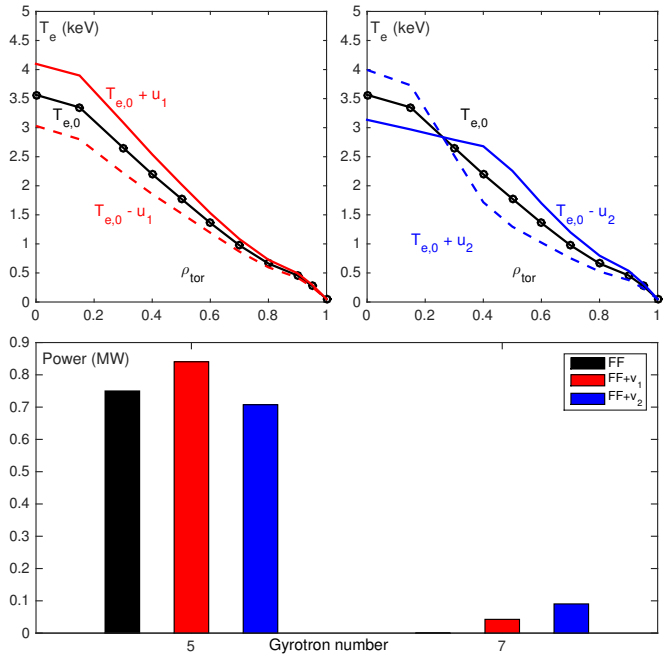

Figure 6. Principal output directions following SVD analysis of the steady-state response of the model to actuator perturbations. Top panels show the first (red) and second (blue) response directions of the $T_e(\rho_{tor})$ profile. The bottom panel shows the corresponding input directions for the two gyrotrons utilized.

The overall controller for the nonlinear system is obtained by adding the feedforward command, the reference, and implementing anti-windup techniques to avoid large differences between controller output and actuator commands in case of saturations. The complete

§ It should be noted that since the chosen operating point has zero power for the second actuator, only a change in the positive direction is physically realizable. However this does not pose a problem in practice if the disturbance to the system (the change in NBI power distribution) appears such that a positive power from that second ECRH actuator is needed to compensate, which is indeed the case here.

diagram of the controller is shown in Figure 7. Overall, the linear controller is written as

$$u_k = C_c x_k^c + D_c e_k + u_{\mathrm{ff}} \tag{3}$$

$$x_{k+1}^c = A_c x_k^c + B_c e_k + K_{\mathrm{aw}}(u_{k,\mathrm{sat}} - u_k) \tag{4}$$

$$z_k = T_o e_k \tag{5}$$

where e_k is the error vector $e_k = (\bar{T}_{e,k} - \bar{T}_{e,\mathrm{ref}})$. u_{ff} is the feedforward input. x_k^c is the controller state, which has no direct physical meaning but is related to integrating elements and other dynamic components of the controller. The last equation gives the controlled variables z_k for analysis purposes. These are obtained by projecting the error onto the principal controllable error directions. The controller matrices $A_c, B_c, C_c, D_c, T_o, K_{\mathrm{aw}}$ are a result of the controller design process. Dimensions of these matrices, together with other details of the controller design, are given in Appendix A.

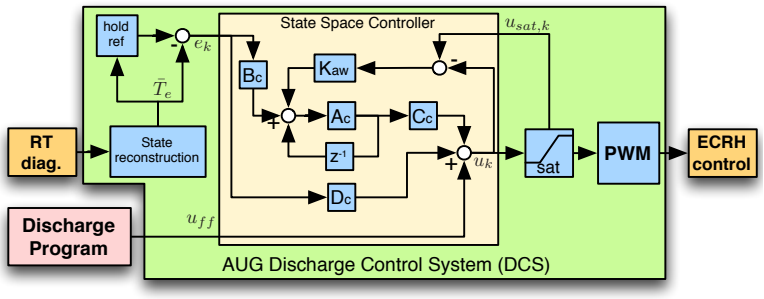

Figure 7. Detail of controller implementation in DCS including saturation, feedforward power command and Pulse-Width Modulation (PWM). The algorithms used for T_e profile reconstruction are gathered in the *state reconstruction* block.

3.5. Closed-loop control simulations using RAPTOR

As a final verification step, the controller is tested in closed-loop with the nonlinear RAPTOR predictive simulation described in Section 3.2. This test is set up to mimic the entire plasma experiment to be performed, including the switch from off- to on-axis NBI and switch from feedforward-only to feedback control. The expected delays in the closed-loop, listed in Table 2.2.4 are also included in the simulation.

The results of this closed-loop simulation are shown in Figure 8. The top panel shows the evolution of plasma current and averaged density, as well as the power of the co or counter-injecting NBI sources, that are given as external input to the simulation. The second panel shows the time traces of the 4 ECRH sources used in this shot, two of which (G6, G8) were feedforward-controlled while two others (G5,G7) were controlled in feedback by the (simulated) T_e profile controller. The third panel shows the temperature values at several radial points, including the reference values obtained by holding the T_e profile values as the controller switch-on time (at 2.8s, marked as the beginning of the gray shaded area) in the bottom panel. This panel also shows the controlled variables corresponding to the projection of the profile error on the two principal directions that are being controlled.

To account for uncertainty in the model, the feedforward-controlled power evolution for ECRH G6 (not controlled in feedback) is set up so that the feedback actuators are saturated during the first part of the on-axis phase, but become de-saturated during the second half. This improves the chance that some part of the on-axis phase control will be successful even if the confinement has been over-estimated in the model. Overall, the closed-loop simulation shows a good closed-loop response within the capabilities of the actuators, which become saturated in some phases of the simulated discharge.

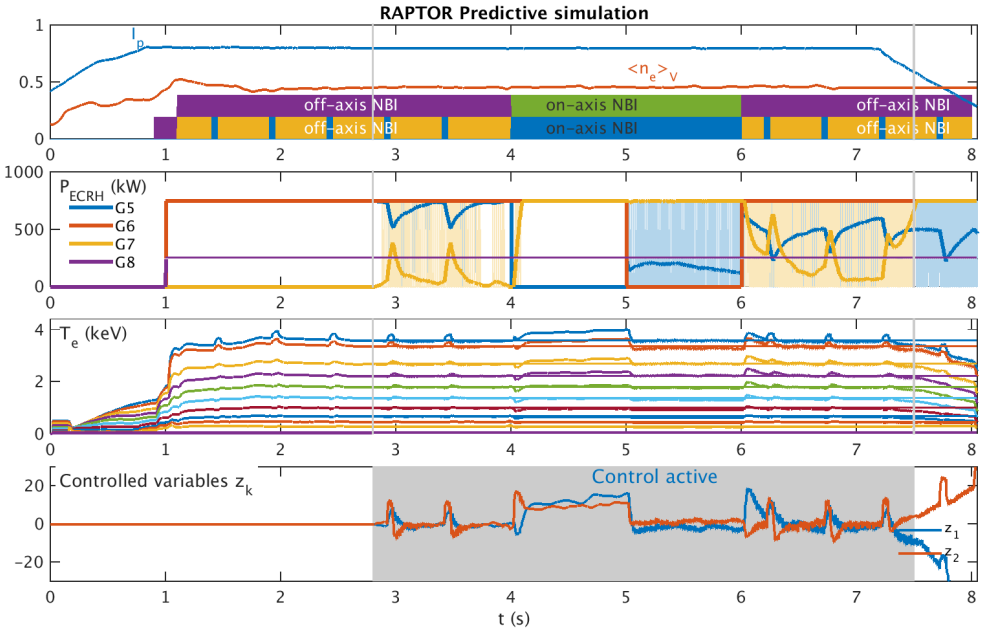

Figure 8. Closed-loop simulation of the shot using the RAPTOR (nonlinear) simulator with the designed controller. Two gyrotrons (G5,G7) are controlled in feedback, and are seen to attempt to compensate disturbances caused by changes between on and off-axis NBI power. The feedforward controlled gyrotron powers (G6,G7) are chosen so as to help the feedback controller. In the phase between 4 and 5 seconds, the feedback-controlled gyrotrons are saturated, hence the target references are not reached.

4. Experimental results

Following the successful closed-loop simulation tests, the controller was implemented in the control framework of the ASDEX-Upgrade DCS system and tested in plasma experiments. The result of the very first attempt at using the controller are shown in Figure 9. As can be observed, the results are very close to the earlier closed-loop simulation results. Saturation of the gyrotron power in some phases of the discharge can be observed, depending on the settings of the feedforward-controlled gyrotrons. Also, due to limited cryo-pump capacity on the day of the experiment, it proved impossible to maintain the desired density, constant even without fuelling, resulting in a slowly increasing plasma density. Towards the end of the shot, this meant that the required temperature could not be maintained by the available feedback-controlled gyrotron power. Some oscillations can be seen in the feedback-controlled phases, which indicates that either the delays were longer than modeled, or other unmodeled plasma or actuator dynamics are at play. It is expected that the oscillations can be reduced by reducing the controller gain, at the expense of a slower response of the closed-loop.

The effect of the controller on the profiles can be seen in 10. Here, the time-averaged temperature profiles estimated by RAPTOR (that are fed to the controller) are shown, together with ECE data constraining the estimates. The left panel shows the time-averages over periods of the shot during which the feedback control was successful. The right panel shows averages over the times when saturation of the actuators resulted in poor control. Also shown are the ECRH power density distributions averaged in the various phases (computed by TORBEAM [32], indicating the effort of the controller to change ECRH power distribution in order to compensate the change in NBI power deposition profiles.

Overall, the control experiment was successful within the limits of the feedback-controllable actuator capacity and plasma conditions.

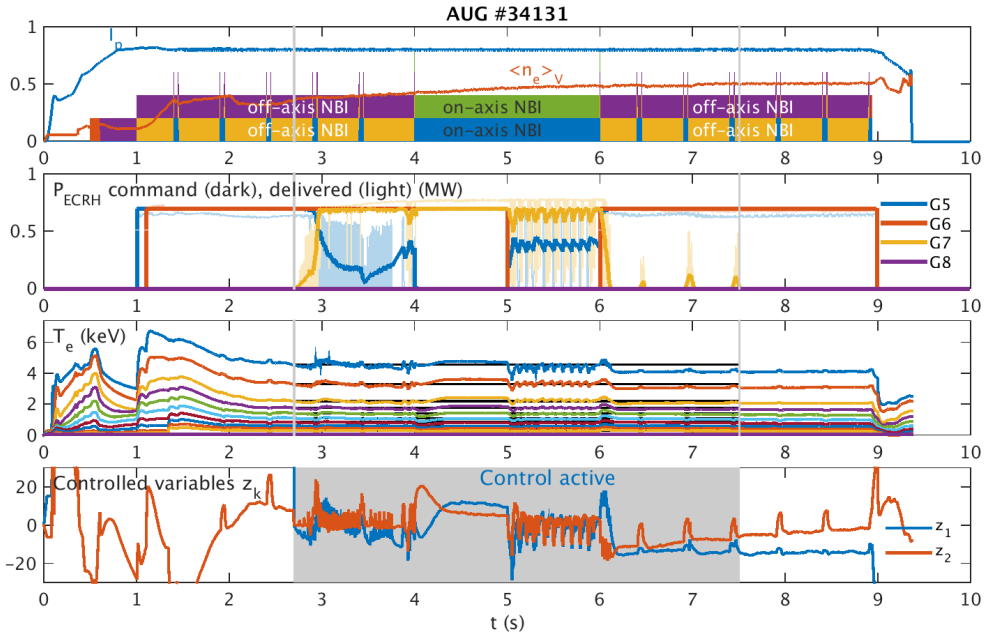

Figure 9. Results of the first shot on AUG using the temperature profile controller. First panel: plasma current, volume averaged density and NBI heating power (feedforward controlled). Second panel: ECRH power command per gyrotron, and estimate of power delivered via Pulse-Width Modulation. Third panel: T_e values estimated by RAPTOR at various rho values, as well as references. Fourth panel: two controlled variables corresponding to the error along the principal control directions. During the phase between feedback switch-on at 2.7s and 4.0s, as well as the interval 5.0s – 6.0s, the gyrotron powers were not saturated and good control was achieved.

5. Conclusions

This work has shown the design methodology and first results of a multi-variable temperature profile controller for the ASDEX-Upgrade tokamak. The controller was designed around a pre-set operating point, based on a linear model of the plasma response to the actuator obtained from the RAPTOR transport code. Following a standard approach in multivariable control design, the controller attempted to control two dominant controllable directions of the temperature profile, that could most be affected most easily by the actuators. Closed-loop simulations were done to verify the controller design, followed by a successful first experimental test on an ASDEX-Upgrade discharge. Within the technical limits of the feedback control, which had only a limited amount of gyrotrons available, the test was successful.

Further work can be envisaged to extend the operating range of the feedback controller. First, making more actuators available to the controller would make it possible to compensate for larger disturbances in density and NBI power. This requires a modification (which is presently underway) of the ASDEX-Upgrade DCS system to enable multiple actuators to be controlled, and dynamically shared, between various controllers. Oscillations that were observed in the feedback-controlled gyrotron power can be alleviated by reducing the controller gains, at the probable expense of reducing the closed-loop bandwidth of the controller.

A recent upgrade of the RAPTOR code to include density profile simulations [33] facilitate the design of multiple controllers for several different conditions (e.g. at different densities density, ECRH deposition location). Then, the resulting controller gains can be parametrized and adapted during the discharge to have the appropriate controller for a variety of operating conditions. In particular, since the temperature response of the temperature to the power

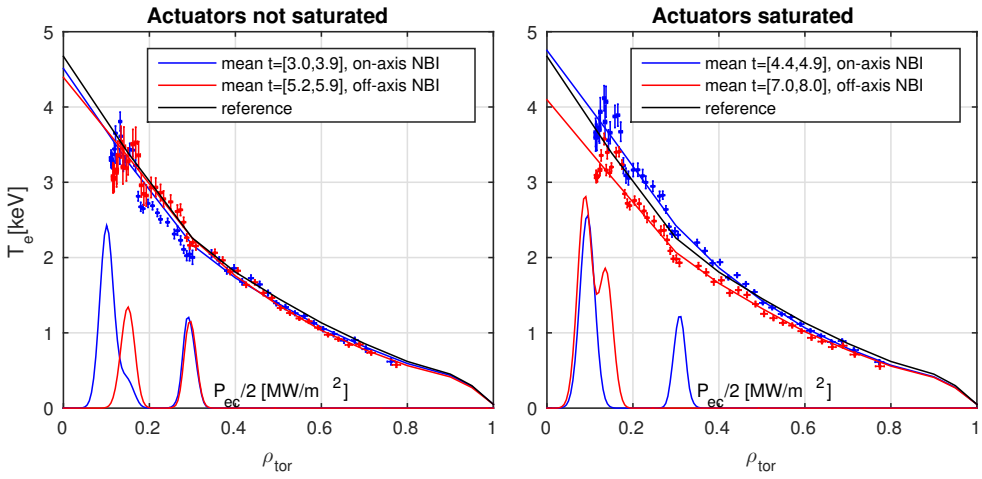

Figure 10. Time-averaged T_e profile estimates from RAPTOR-observer (solid) and ECE measurements (symbols) during various phases in shot #34131, together with time-averaged ECRH power distributions. Left: On-axis and off-axis NBI phases where ECRH actuators were not saturated and T_e control was successful. Right: NBI periods where actuators were saturated and the targets profile could not be achieved. Errorbars on ECE measurements indicate the standard deviation during the time interval considered. ρ_{tor} values for ECE measurements computed from the real-time equilibrium and correspond to what is known to the RAPTOR-observer in real-time.

scales approximately inversely with density, scaling the controller gains linearly with density seems a reasonable approach to be able to use the controller over a variety of density regimes.

Also, while the present controller was aimed at controlling (parameters of) the temperature profile, it is certainly possible to extend the design procedure to control other parameters of interest. For example the temperature gradient (averaged over a region of interest), or the peak temperature can be controlled or quantities related to the ion temperature profile if that can be measured in real-time.

Finally, in view of ITER and other long-pulse tokamaks, a kinetic controller such as the one shown in this paper should be embedded in a real-time plasma supervision and actuator management scheme e.g. [34], [35] that enables and prioritizes control targets for the controller in real-time, as well as dynamically assigning actuators and setting actuator limits to the controller.

Appendix A. Details of MIMO-SVD controller design and anti-windup

Appendix A.1. Principal control direction

We start with a continuous-time LTI MIMO plant $P(s)$ (here s is the Laplace operator) describing the system to be controlled, obtained from the local linearization of the system around an operating point. This plant has n_u inputs and n_y outputs, where we assume $n_y \leq n_u$ (more outputs than inputs, as is typically the case when controlling many points of a profile with only few actuators). In this case it is not possible to control the outputs of P individually. We choose therefore to control only certain dominant "directions" in the output vector space. These directions are determined by an SVD, using a standard technique described e.g. in [36].

We first scale the inputs and outputs to have roughly the same order of magnitude using (diagonal) matrices S_i and S_o, and apply (optionally) a diagonal output weighting matrix W_o to weigh the importance of various outputs for control (for example, preferentially control the profile in a given radial region of the plasma). The scaled and weighted matrix becomes: $P_s(s) = W_o S_o P(s) S_i$. The controller decoupling is based on the value of $P(s = j\omega)$ at $\omega = 0$, corresponding to the DC gain or static response of the system, but other choices are possible.

Let $P_o = P(0) \in \mathbb{R}^{n_y \times n_u}$ be the matrix describing the gain relations between inputs and outputs at that frequency. Similarly we define $P_{so} = P_s(0) \in \mathbb{R}^{n_y \times n_u}$.

We then take the SVD of the P_{so} matrix. $U\Sigma V^T = P_{so}$, and choose to control only n_u output directions of the plant. For this purpose we partition U as $U\Sigma V^T = \begin{bmatrix} U_1 & U_2 \end{bmatrix} \Sigma V^T$ with $U_1 \in \mathbb{R}^{n_y \times n_u}$, $\Sigma \in \mathbb{R}^{n_u \times n_u}$ and $V^T \in \mathbb{R}^{n_u \times n_u}$. Noticing that $(V\Sigma^{-1}U_1^T)$ is the Pseudoinverse of P_{so} it holds that $(V\Sigma^{-\frac{1}{2}})(\Sigma^{-\frac{1}{2}}U_1^T)P_{so} = (V\Sigma^{-1}U_1^T)P_{so} = I_{n_u}$. Defining $V_o = V\Sigma^{-\frac{1}{2}}$, $U_o^T = \Sigma^{-\frac{1}{2}}U_1^T$ we get $V_o U_o^T P_{so} = I$.

Multiplying from the left by V_o^T and from the right by V_o we get $U_o^T P_{so} V_o = I_{n_u}$. Now we can define the decoupled dynamical plant

$$P_d(s) = U_o^T P_s(s) V_o = U_o^T (W_o S_o P(s) S_i) V_o \tag{A.1}$$

Which will obviously have DC gain $P_d(0) = I_{n_u}$. For this plant, at low frequency, input i will dominantly affect output i and the effect on other outputs will be small.

For notational simplicity we finally define $T_o = U_o^T W_o S_o$ and $T_i = S_i V_i$, so that

$$P_d(s) = T_o P(s) T_i \tag{A.2}$$

Finally a time delay of 14ms is added following the delay budget specified in Table 2.2.4. The four transfer functions describing this (2×2) system are shown in Figure A1 (blue curves), confirming that the off-diagonal terms are much smaller than the dominant diagonal terms.

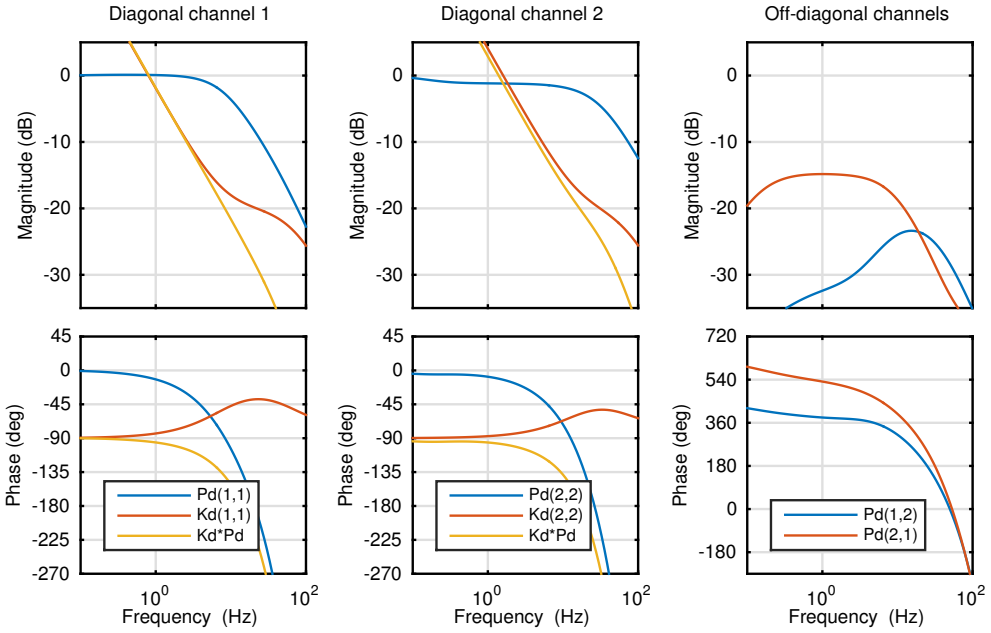

Figure A1. Bode plots of the plant model and controller including a loop delay of 14ms. Left panels: First diagonal element $P_d(1,1)$, SISO controller $K_d(1,1)$ and corresponding open loop $P_d(1,1)K_d(1,1)$. Middle panels: Second diagonal element $P_d(2,2)$, SISO controller $K_d(2,2)$ and corresponding open loop $P_d(2,2)K_d(2,2)$. Right panels: Off-diagonal elements $P_d(2,1)$ and $P_d(1,2)$. Note that the off-diagonal entries for K_d are zero.

Appendix A.2. Controller design

We now design a dynamic controller $K_d(s)$ for the decoupled system $P_d(s)$. Since the system is decoupled at low frequency ($P_d(0) = I$), we seek a *diagonal* controller $K_d(s)$ with SISO controllers $k_i(s)$ on the diagonal for $i = [0, \ldots, n_u]$. The design of each $k_i(s)$ controller can be done using standard SISO loop-shaping or PID tuning techniques. The result is first checked on the individual (decoupled loops), then on the coupled system to check for any residual coupling

effects. The two controller transfer functions for the diagonal elements are shown in A1 together with the corresponding open-loop transfer functions. One can see that the gains are chosen quite low, yielding a conservative controller with low bandwidth and predominantly integral action. For a first test of the controller, this was deemed an appropriate choice. A rolloff term is also added to eliminate high-frequency responses of the controller. The magnitude of the closed-loop sensitivity functions, defined as $S = 1/(I + P_d K_d)$ from the two references to the two errors are shown in Figure A2, confirming that low-frequency errors are rejected and off-diagonal response is small.

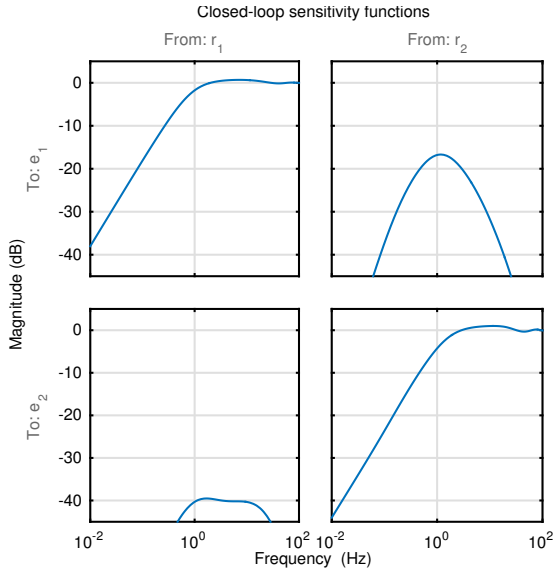

Figure A2. Magnitudes of closed-loop sensitivity with the diagonalized controller. These represent the frequency response of the error when applying a sinusoidal signal on one of the control references. As expected, low-frequency errors are rejected up to the bandwidth of the closed-loop. The off-diagonal sensitivities, representing cross-coupling between the control channels, remain small.

Once the controller $K_d(s)$ for $P_d(s)$ has been designed, it is transformed into a controller $K(z)$ for $P(z)$ as follows:

$$K(s) = T_i K_d(s) T_o \tag{A.3}$$

The interconnection relations in the feedback loop are: $U(s) = K(s)E(s)$, $E(s) = R(s) - Y(s)$, $Y(s) = P(s)U(s)$, with $U(s)$ the (Laplace transform of the) input to the plant, $Y(s)$ the output of the plant, $R(s)$ the reference, and $E(s)$ the error. This MIMO controller is finally formulated in a discrete-time state space realization of the form $[A_K, B_K, C_K, D_K]$, after choosing a sufficiently small sampling frequency w.r.t. the closed-loop bandwidth. The controller can be simulated using the familiar state-space equations, adding an extra feedforward term:

$$x_{k+1} = A_K x_k + B_K e_k \tag{A.4}$$

$$u_k \quad = C_K x_k + D_K e_k + u_{ff,k} \tag{A.5}$$

where u_k is the vector of outputs of the controller (the control signal to the plant). e_k is the input to the controller: the vector of tracking errors. x_k is the internal state of the (dynamic) controller. $u_{ff,k}$ is a feedforward input signal. Additional terms are added to the controller to implement anti-windup compensation, ensuring the controller state remains congruent with the true (saturated) input signal, following standard techniques described in [37].

An additional equation can be written for the n_u-dimensional controlled variable. This is added as an output of the controller to be able to assess the effect of the control action.

$$z_k = T_o e_k \tag{A.6}$$

Acknowledgements

This work has been carried out within the framework of the EUROfusion Consortium and has received funding from the Euratom research and training programme 2014-2018 under grant agreement No 633053. The views and opinions expressed herein do not necessarily reflect those of the European Commission. This work was supported in part by the Swiss National Science Foundation.

References

[1] Albanese, R. *et al.* 2005 *Fusion Engineering and Design* **74** 627
[2] Katsuro-Hopkins, O. *et al.* 2007 *Nuclear Fusion* **47** 1157
[3] Moreau, D. *et al.* 2015 *Nuclear Fusion* **55** 63011
[4] Barton, J. *et al.* 2015 *Nuclear Fusion* **55** 093005
[5] Maljaars, E. *et al.* 2017 *Fusion Engineering and Design*
[6] Boyer, M.D. *et al.* 2014 *Plasma Physics and Controlled Fusion* **56** 104004
[7] Humphreys, D. *et al.* 2015 *Physics of Plasmas* **22**
[8] de Vries, P. *et al.* 2018 *Fusion Engineering and Design* **129** 334
[9] Kim, H.S. *et al.* 2018 *Fusion Engineering and Design* **135** 1
[10] Moreau, D. *et al.* 2013 *Nuclear Fusion* **53** 063020
[11] Boyer, M.D. *et al.* 2017 *Nuclear Fusion* **57** 066017
[12] Kim, S. *et al.* 2012 *Nuclear Fusion* **52** 074002
[13] Wehner, W. *et al.* 2016 in *2016 IEEE Conference on Control Applications (CCA)* IEEE ISBN 978-1-5090-0755-4 629–634
[14] Argomedo, F.B. *et al.* 2013 *Nuclear Fusion* **53** 033005
[15] Vu, N.T. *et al.* 2017 *Fusion Engineering and Design* **123** 624
[16] Mavkov, B. *et al.* 2018 *Nuclear Fusion* **58** 056011
[17] Felici, F. *et al.* 2012 *Plasma Physics and Controlled Fusion* **54** 025002
[18] Felici, F. *et al.* 2011 *Nuclear Fusion* **51** 083052
[19] Geiger, B. *et al.* 2015 *Nuclear Fusion* **55** 083001
[20] Fischer, R. *et al.* 2010 *FUSION SCIENCE AND TECHNOLOGY* **58** 675
[21] Treutterer, W. *et al.* 2014 *Fusion Engineering and Design* **89** 146
[22] Reich, M. *et al.* 2010 *Fusion Science and Technology* **58** 727
[23] Giannone, L. *et al.* 2015 *Fusion Engineering and Design* **100** 519
[24] Felici, F. *et al.* 2016 in *26th IAEA Fusion Energy Conference, Kyoto, Japan* EX/P8–33
[25] Teplukhina, A.A. *et al.* 2017 *Plasma Physics and Controlled Fusion* **59** 124004
[26] Erba, M. *et al.* 1998 *Nuclear Fusion* **38** 1013
[27] Blanken, T.C. *et al.* 2018 *Fusion Engineering and Design* **126** 87
[28] Felici, F. *et al.* 2014 in *2014 American Control Conference* IEEE, Portland, Oregon ISBN 978-1-4799-3274-0 4816–4823
[29] Rathgeber, S.K. *et al.* 2013 *Plasma Physics and Controlled Fusion* **55** 025004
[30] Budny, R.V. *et al.* 2008 *Nuclear Fusion* **48** 75005
[31] Barton, J.E. *et al.* 2015 *Plasma Physics and Controlled Fusion* **57** 115003
[32] Poli, E. *et al.* 2018 *Computer Physics Communications* **225** 36
[33] Felici, F. *et al.* 2018 *Nuclear Fusion* **58** 096006
[34] Eidietis, N. *et al.* 2018 *Nuclear Fusion* **58** 056023
[35] Maljaars, E. *et al.* 2017 *Nuclear Fusion* **57** 126063
[36] Skogestad, S. *et al.* 2005 *Multivariable Feedback Control* John Wiley & Sons Ltd.
[37] Åstrom, K.J. *et al.* 1997 *Computer-Controlled Systems: theory and design* Prentice Hall, Upper Saddle River, New Jersey third edition